

Article

Improved Polymer Crystal Phase Field Model and Numerical Simulation

Binxin Yang *, Zhifeng Wang and Zhijuan Meng

School of Applied Science, Taiyuan University of Science and Technology, Taiyuan 030024, China

* Correspondence: binxinyang@tyust.edu.cn

Abstract: The existing phase field model of polymer crystallization contains many parameters that lack actual physical meaning. Although the value of these parameters can be adjusted to obtain results consistent with the experiment, it cannot correspond to the experimental conditions. In this paper, a new phase field model is established. By adjusting the latent heat, various forms of isotactic polystyrene crystals, such as dendrites, spherulites, lamellas, etc., can be simulated. Latent heat refers to the heat absorbed or released by a substance from one phase to another and has important physical meaning during the solidification process. The finite difference method was used to solve the model, and then the data were used to visualize. The simulation results were consistent with the experiment. Numerical simulation results under pure diffusion conditions show that the newly established phase field model can qualitatively predict the polymer growth process and provide a theoretical basis for the preparation and optimization of high-performance polymers. In order to make the simulation result closer to the actual growth of the crystal, the flow velocity is added in the simulation to make the melt convection. Under forced convection, the simulated polymer crystal image is no longer symmetrical.

Keywords: phase field model; latent heat; polymer; numerical simulation; finite difference method; convection

MSC: 76-10

Citation: Yang, B.; Wang, Z.; Meng, Z. Improved Polymer Crystal Phase Field Model and Numerical Simulation. *Mathematics* **2022**, *10*, 3181. <https://doi.org/10.3390/math10173181>

Academic Editors: Peng-Nan Sun, Tao Jiang and Junseok Kim

Received: 10 August 2022

Accepted: 30 August 2022

Published: 3 September 2022

Publisher's Note: MDPI stays neutral with regard to jurisdictional claims in published maps and institutional affiliations.



Copyright: © 2022 by the authors. Licensee MDPI, Basel, Switzerland. This article is an open access article distributed under the terms and conditions of the Creative Commons Attribution (CC BY) license (<https://creativecommons.org/licenses/by/4.0/>).

1. Introduction

With the development of materials science, polymers have become indispensable materials in our lives. The microstructure formed during the solidification process determines the properties of the polymer. In the early days, experimental methods were often used to study microstructures. Due to the influence of experimental conditions, costs, and the rapid development of computer science, numerical simulation methods were often used in the later stages to study microstructures [1]. Crystallization is a phase transformation of matter from an amorphous to a crystalline state. In general, crystallization involves two steps: nucleation and growth [2]. Since the phase field method avoids the tracking interface, on the basis of generating punctate nuclei or directional nuclei, this paper uses the phase field method to numerically simulate the growth process of isotactic polystyrene. Caginalp [3] verified the phase field model, confirmed the correctness of the model, and introduced anisotropy into the model. R. Kobayashi [4] used an anisotropic phase field model to perform two-dimensional numerical simulation of dendrites, and later he extended the dimension to three-dimensional. However, the early phase field model does not conform to the principle of the local entropy increase in thermodynamics. Gránásy et al. [5,6] used artificially specified parameters in the phase field model and did not obtain the parameters from the real material, which is not conducive to linking the simulation results with the experiment. Xu et al. [7] established a phase field model with polymer characteristics and extracted model parameters from actual material parameters so that the phase field

variables had practical significance. Based on the local free energy function proposed by Harrowell and Oxtoby [8], Wang et al. [9] improved the phase field governing equation of Xu et al. Zhang et al. [1] found that when $T_c \geq 230\text{ }^\circ\text{C}$, the value of ζ constructed by Wang et al. fluctuates greatly and even appeared negative. Therefore, the free energy density function is reconstructed, and the phase field governing equation is established. In this paper, the phase field equation improved by Zhang et al. is coupled with the temperature field equation improved by Bahloul A et al. [10] to establish a phase field model. By changing the latent heat, various forms of isotactic polystyrene crystals, such as dendrites, spherulites, lamellas, etc., can be simulated. The crystal evolution is controlled by two equations; one is the phase field equation that controls the crystal evolution, and the other is the heat equation that controls the temperature [10].

2. Phase Field Model

2.1. Phase Field Equation

The phase field equation introduces the variable $\Phi(x, t)$ to represent the physical state of the system in space x and time t . $\Phi(x, t)$ is a dimensionless variable, $\Phi = 1$ means solid phase, and $\Phi = 0$ means liquid or amorphous phase. On the solid–liquid interface, Φ changes continuously between 0 and 1. The equation of $\Phi(x, t)$ evolving with time is:

$$\frac{\partial\Phi(x, t)}{\partial t} = -\Gamma \frac{\delta F(\Phi, T)}{\delta\Phi(x, t)} \tag{1}$$

Among them, $\Phi(x, t)$ is a non-conservative phase field variable, Γ is the interface mobility, $F(\Phi, T)$ is the total free energy of the system, and the expression is:

$$F(\Phi, T) = \int f_{cryst}(\Phi, T)dV = \int [f_{cryst}(\Phi, T) + f_{grad}(\Phi)]dV \tag{2}$$

$f_{local}(\Phi, T)$ represents the local free energy density function, and $f_{grad}(\Phi)$ represents the gradient free energy function. Wang et al. improved the phase field governing equation of Xu et al. based on the local free energy function proposed by Harrowell and Oxtoby. The expression is as follows:

$$\frac{\partial\Phi(x, t)}{\partial t} = -\Gamma[W\Phi(\Phi - \zeta) - k_0^2\nabla \cdot (\beta(\theta)^2) + k_0^2 \frac{\partial}{\partial x}(\beta(\theta)\beta'(\theta)) \frac{\partial\Phi}{\partial y} + k_0^2 \frac{\partial}{\partial y}(\beta(\theta)\beta'(\theta)) \frac{\partial\Phi}{\partial x}] \tag{3}$$

Zhang et al. found that when $T_c \geq 230\text{ }^\circ\text{C}$, the value of ζ constructed by Wang et al. fluctuates greatly and even appears negative. This is obviously unreasonable. Since the values of ζ and Φ will have a great impact on the free energy density function, in order to simulate the crystal growth phenomenon more reasonably, when $T_c \geq T_m$ and $T_c < T_m$, Zhang et al. modified Φ and ζ . The free energy density function is reconstructed, and the phase field governing equation is established. The expression is as follows:
when $T_c < T_m$:

$$\zeta = \frac{1}{2}\zeta_0 - \frac{3\zeta_0^2 - 6\zeta_0\hat{\Phi} + 3\hat{\Phi}^2}{6\zeta_0 - 4\hat{\Phi}}, \hat{\Phi} = \frac{T_m^0 - T_m}{T_m^0 - T} \tag{4}$$

when $T_c \geq T_m$:

$$\zeta = \frac{1}{2}\zeta_0 + \frac{3\zeta_0^2 - 6\zeta_0\hat{\Phi} + 3\hat{\Phi}^2}{6\zeta_0 - 4\hat{\Phi}}, \hat{\Phi} = \frac{T_m^0 - T_m}{T_m^0 - 2(T_m - T)} \tag{5}$$

2.2. Temperature Field Equation

2.2.1. Traditional Temperature Field Equation

During the crystallization process, the crystallization rate and morphology of polymer crystals are affected by many factors, such as latent heat, flow velocity, etc. The equation for the evolution of the temperature field $T(x, t)$ with time is :

$$\frac{\partial T}{\partial t} = \alpha \nabla^2 T + K \frac{\partial \Phi}{\partial t} \tag{6}$$

Among them, the thermal diffusivity is $\alpha = \frac{k}{\rho C_p}$, $K = \frac{\Delta H}{C_p}$, ρ means density, ΔH means latent heat, and C_p means specific heat capacity at constant pressure.

2.2.2. The Improved Temperature Field Equation of Bahloul A et al.

Since the phase field variable $\frac{\partial \Phi}{\partial t}$ is proportional to the propagation velocity v_n of the interface, the evolution of $\frac{\partial \Phi}{\partial t}$ and the front growth rate G_r are similar [10]. Based on this idea, Bahloul A et al. combined the phase field equation of the growth equation proposed by Lauritsen and Hoffmann [11,12] and set the dimensionless diffusion coefficient $\tau = \frac{\alpha}{\epsilon^2 \Gamma}$ between T_{cmax} and T_m^0 to: $\tau^* = \frac{1}{H(T_c)}$, and the dimensionless latent heat K between T_g and T_{cmax} is modified to: $K^* = \frac{\hat{K}_0}{H(T_c)}$. At other temperatures $\tau^* = 1$, $K^* = \hat{K}_0$. The model parameters are all calibrated under T_{cmax} , and the temperature dependence is only represented by $H(T_c)$. The expression of $H(T_c)$ is as follows:

$$H(T_c) = h_0 \exp\left(-\frac{h_1}{T_c - 60}\right) \exp\left(-\frac{h_2}{242 - T_c}\right) \tag{7}$$

Among them, T_c represents the experimental temperature, T_g represents the glass transition temperature, T_{cmax} represents the maximum growth temperature, \hat{K}_0 represents the initial dimensionless latent heat, h_1 and h_2 are parameters, and only the following conditions are required:

$$H(T_c = T_{cmax}) = 1, \frac{dH(T_c)}{dT_c}(T_c = 180 \text{ }^\circ\text{C}) = 0, h_0 = \exp\left(\frac{h_1 + h_2 + 2\sqrt{h_1 h_2}}{62}\right) \tag{8}$$

In this paper, for the convenience of calculation, $h_0 = 1.0378$, $h_1 = 3.75$, and $h_2 = 1$, respectively. The improved temperature field equation is:

$$\frac{\partial T}{\partial t} = \alpha \nabla T^2 + K^* \frac{\partial \Phi}{\partial t} \tag{9}$$

Based on the improved phase field equations of Zhang et al., this paper couples the improved temperature field equations of Bahloul A et al. to establish a new phase field model. The governing equations are as follows:

$$\frac{\partial \Phi}{\partial t} = -\Gamma [W\Phi(\Phi - \frac{\xi_0}{2} + \hat{\xi}) - k_0^2 \nabla \cdot (\beta^2(\theta)) \nabla \Phi + k_0^2 \frac{\partial}{\partial x} (\beta(\theta)\beta'(\theta) \frac{\partial \Phi}{\partial y}) - k_0^2 \frac{\partial}{\partial y} (\beta(\theta)\beta'(\theta) \frac{\partial \Phi}{\partial x})] \tag{10}$$

$$\frac{\partial T}{\partial t} = \alpha \nabla T^2 + K^* \frac{\partial \Phi}{\partial t}$$

2.3. Numerical Solution of Phase Field Model

In the process of numerical solution, the area to be solved is meshed first, and then the phase field equations and temperature field equations are discretized at nodes so that the equations are only established at discrete nodes [13]. Finally, the discretization method is used on the nodes, the numerical solution is used as the approximate value of the exact solution, and the difference format is obtained.

The finite difference method is used to numerically solve the phase field model. In order to facilitate the calculation, the variables are dimensionless. The first-order partial derivatives of $\Phi(x, t)$ and $T(x, t)$ with respect to time both use forward differences and the partial derivatives of $\Phi(x, t)$ with respect to space use second-order central differences. The nine-point difference format is used for Laplacian $\nabla^2\Phi, \nabla^2T$.

$$\frac{\partial\Phi}{\partial t}\Big|_{i,j}^n \approx \frac{\Phi_{i,j}^{n+1} - \Phi_{i,j}^n}{\Delta t} \tag{11}$$

$$\frac{\partial T}{\partial t}\Big|_{i,j}^n \approx \frac{T_{i,j}^{n+1} - T_{i,j}^n}{\Delta t} \tag{12}$$

$$\frac{\partial^2\Phi}{\partial x^2}\Big|_{i,j}^n \approx \frac{\Phi_{i+1,j}^n - 2\Phi_{i,j}^n - \Phi_{i-1,j}^n}{\Delta x^2} \tag{13}$$

$$\frac{\partial^2\Phi}{\partial y^2}\Big|_{i,j}^n \approx \frac{\Phi_{i,j+1}^n - 2\Phi_{i,j}^n - \Phi_{i,j-1}^n}{\Delta y^2} \tag{14}$$

$$\begin{aligned} \nabla^2\Phi = \left(\frac{\partial^2\Phi}{\partial x^2} + \frac{\partial^2\Phi}{\partial y^2}\right) &\approx \frac{2\Phi_{i+1,j}^n + 2\Phi_{i-1,j}^n + 2\Phi_{i,j-1}^n + 2\Phi_{i,j+1}^n - 12\Phi_{i,j}^n}{4\Delta x^2} \\ &+ \frac{\Phi_{i+1,j-1}^n + \Phi_{i-1,j-1}^n + \Phi_{i+1,j+1}^n + \Phi_{i-1,j+1}^n}{4\Delta x^2} \end{aligned} \tag{15}$$

$$\begin{aligned} \nabla^2T = \frac{\partial^2T}{\partial x^2} + \frac{\partial^2T}{\partial y^2} &\approx \frac{2T_{i+1,j}^n + 2T_{i-1,j}^n + 2T_{i,j-1}^n + 2T_{i,j+1}^n - 12T_{i,j}^n}{4\Delta x^2} \\ &+ \frac{T_{i+1,j-1}^n + T_{i-1,j-1}^n + T_{i+1,j+1}^n + T_{i-1,j+1}^n}{4\Delta x^2} \end{aligned} \tag{16}$$

Since the phase field model only gives the evolution of the liquid–solid interface, initial conditions are required: the radius of the crystal nucleus is r_0 , the internal phase field parameter of the nucleation $\phi = \zeta_0$, the external phase field parameter of the nucleation $\phi = 0$, and the initial temperature is $T = 0$.

$$\begin{aligned} &\text{when } x^2 + y^2 \leq r_0^2, \Phi = \zeta_0, T = 0 \\ &\text{when } x^2 + y^2 > r_0^2, \Phi = 0, T = 0 \end{aligned}$$

Boundary conditions: At the boundary of the calculation grid, both the phase field and the temperature field use cyclic boundary conditions.

3. Result

Under pure diffusion conditions, the improved phase field model is used to numerically simulate the growth process of isotactic polystyrene (ips), and the numerical results are compared with experimental results to verify the feasibility of the newly established phase field model. The common forms of isotactic polystyrene crystals are: dendrites, spherulites, lamellas, and so on. A numerical simulation is performed on a cell grid with $N_x = N_y = 500$. The spatial steps in the x and y directions are $\Delta x = \Delta y = 3$, and the time step is $\Delta t = 0.1$. The parameters used in the simulation are shown in Table 1.

Table 1. The parameter values required for simulation are shown in the following table.

Parameter	Value
maximum growth temperature T_{cmax}	180 °C
class transition temperature T_g	90 °C
experiment temperature T_c	180 °C
melting temperature T_m	224.7 °C
equilibrium melting temperature T_m^0	242 °C
Initial offset angle θ_0	0
Phase field parameters inside nucleation ξ_0	0.929
Anisotropy modulus j	6
Model parameters W	5.76

Numerical Simulation Results

(1) Dendrite

In the simulation, the initial latent heat is $K_0 = 0.95$, the anisotropy strength is $\epsilon = 0.06$, and the morphology of the dendrite is obtained by the simulation. The result is shown in Figure 1a–c. Their time iteration steps are 1000, 2000, and 3000, respectively. By comparing the results with the experimental result (d), it is found that the numerical simulation results are very consistent with the experimental results.

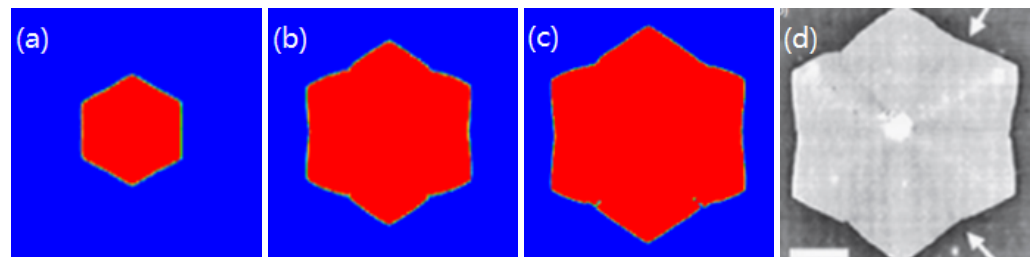


Figure 1. When $K_0 = 0.95$, the morphology of dendrites is obtained by numerical simulation. ((a–c) are the numerical simulation results with time iteration steps of 1000, 2000, and 3000, respectively. (d) is the experimental result).

In the simulation, the initial latent heat is $K_0 = 1.1$, and the anisotropy strength is $\epsilon = 0.06$. The simulation results are shown in Figure 2a–c. Their time iteration steps are 1000, 2000, and 3000, respectively. The simulation obtains a hexagonal snowflake shape. By comparing the results with the experimental result (d), it is found that the numerical simulation result is very close to the experimental result.

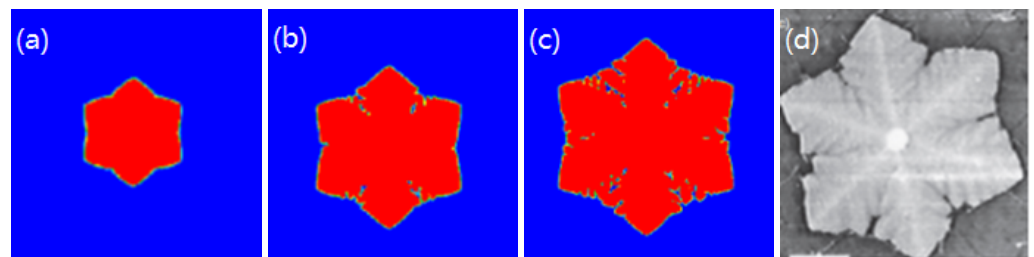


Figure 2. When $K_0 = 1.1$, and the morphology of dendrites is obtained by numerical simulation. ((a–c) are the numerical simulation results with time iteration steps of 1000, 2000 and 3000, respectively. (d) is the experimental result).

In the simulation, the initial latent heat is $K_0 = 1.25$, the anisotropy strength is $\epsilon = 0.06$, and the morphology of the dendrite is obtained by the simulation. The time iteration steps in Figure 3 are 1000, 2000, and 3000, respectively. (a–c) are the numerical results, and (d) is the experimental result. Comparing the numerical simulation results with the experimental results, it is found that they are very close.

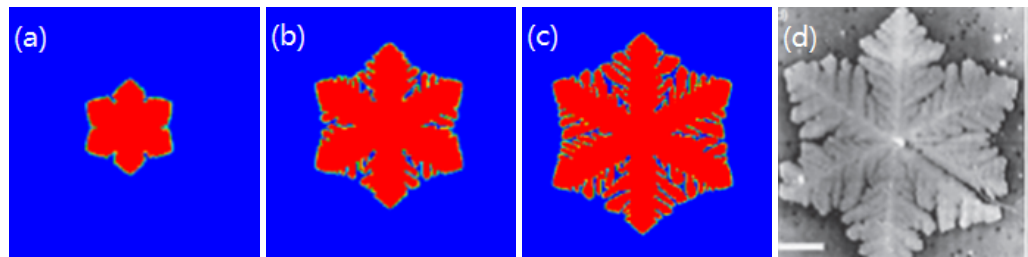


Figure 3. When $K_0 = 1.25$, the morphology of dendrites is obtained by numerical simulation. ((a–c) are the numerical simulation results with time iteration steps of 1000, 2000 and 3000, respectively. (d) is the experimental result).

In the simulation, the initial latent heat is $K_0 = 1.5$, and the anisotropy strength is $\varepsilon = 0.06$. The time iteration steps in Figure 4 are 1000, 3000, and 5000, respectively. (a–c) are the numerical results, and (d) is the experimental result. By comparing the results with the experimental result (d), it is found that the numerical results are almost in good agreement with the experimental results.

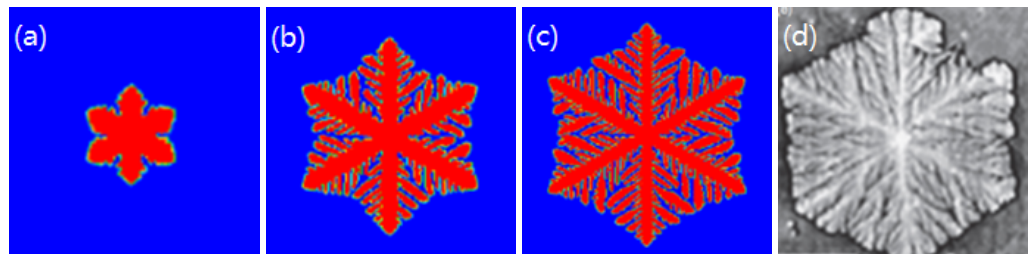


Figure 4. When $K_0 = 1.5$, and the morphology of dendrites is obtained by numerical simulation. ((a–c) are the numerical simulation results with time iteration steps of 1000, 3000 and 5000, respectively. (d) is the experimental result).

(2) Spherulites

In the simulation, the initial latent heat is $K_0 = 1.4$, the anisotropy strength is $\varepsilon = 0$, and the spherulite morphology is obtained by the simulation. The time iterations in Figure 5 are 1000, 3000, and 5000, respectively. (a–c) are the numerical results, and (d) is the experimental result. Through comparison, it is found that the numerical results are very consistent with the experimental results.

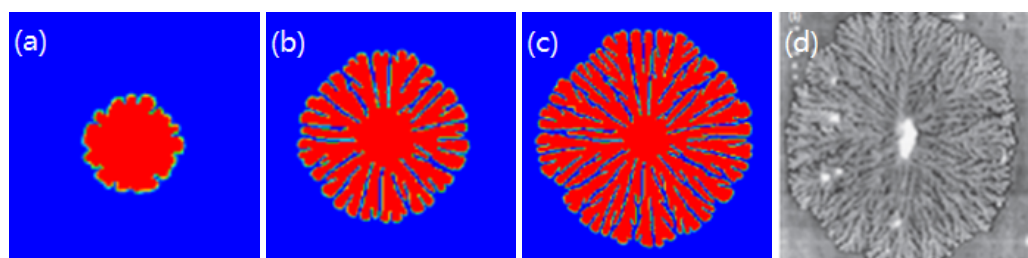


Figure 5. When $K_0 = 1.4$, the morphology of spherulite is obtained by numerical simulation. ((a–c) are the numerical simulation results with time iteration steps of 1000, 3000 and 5000, respectively. (d) is the experimental result).

(3) Lamellar

In the simulation, the initial latent heat is $K_0 = 0.8$, and the anisotropy strength is $\varepsilon = 0.06$. The time iteration steps in Figure 6 are 1000, 3000, and 5000. (a–c) are the numerical results, and (d) is the experimental result. By comparing with the experimental result (d), the numerical result is highly consistent with the experimental result.

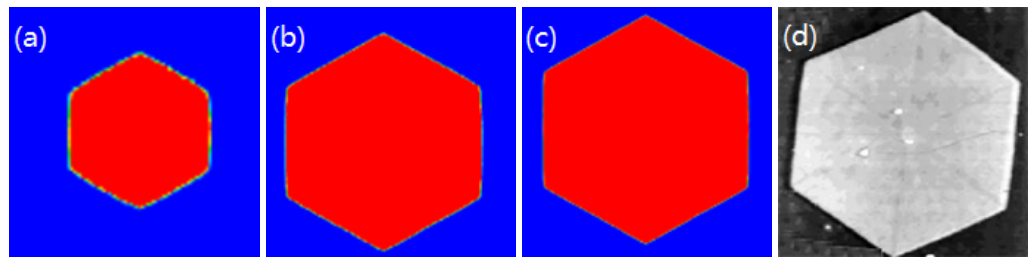


Figure 6. When $K_0 = 0.8$, the morphology of lamellar is obtained by numerical simulation. ((a–c) are the numerical simulation results with time iteration steps of 1000, 3000 and 5000, respectively. (d) is the experimental result).

By analyzing and comparing the simulation results and experimental results of the above figures, it can be concluded that the phase field model established in this paper can qualitatively predict polymer crystallization and provide a theoretical basis for the preparation and optimization of high-performance polymers. The phase field model can simulate various forms of isotactic polystyrene crystals, such as dendrites, spherulites, lamellas, etc., by adjusting the latent heat. Latent heat refers to the heat absorbed or released by a substance from one phase change to another under isothermal and isostatic conditions. Compared with the previous phase field model, latent heat has practical physical meaning.

4. Discussion

4.1. Dynamic Phase Field Model of Polymer Crystallization

In the process of polymer transition from liquid phase to solid phase, the relative flow caused by the temperature difference of various internal parts, that is, convection. Convection is divided into natural convection and forced convection. Natural convection is usually convection generated spontaneously due to density changes caused by concentration differences or temperature differences. Forced convection is usually convection generated by external forces, such as increasing the flow velocity of liquids and gases. Convection mainly affects the distribution of temperature, which in turn affects the shape of the solid–liquid interface. Therefore, convection is crucial to the microstructure formed during the solidification process. In order to make the simulation result closer to the actual polymer growth, speed is added in the simulation to make the melt produce forced convection. The temperature field equation of the coupled flow field:

$$\frac{\partial \phi}{\partial t} = -\Gamma[W\phi(\phi - \frac{\xi_0}{2} + \hat{\xi}) - k_0^2 \nabla \cdot (\beta^2(\theta)) \nabla \phi + k_0^2 \frac{\partial}{\partial x} (\beta(\theta)\beta'(\theta) \frac{\partial \phi}{\partial y}) - k_0^2 \frac{\partial}{\partial y} (\beta(\theta)\beta'(\theta) \frac{\partial \phi}{\partial x})] \quad (17)$$

$$\frac{\partial T}{\partial t} + (1 - \phi)V \cdot \nabla T = \alpha^* \nabla^2 T + k^* \frac{\partial \phi}{\partial t}$$

4.2. String Crystals

The polymer melt first forms a crystal nucleus during the cooling process. The shape of the crystal nucleus initially affects the crystalline morphology of the polymer crystal, and then it affects the mechanical properties of the polymer product. The common crystal nuclei of polymers are divided into point-like nuclei and directional nuclei. The point-like nuclei gradually form spherulites during the growth process. Oriented nuclei form oriented structures during the growth process, such as skeletons that are strongly dependent on orientation during crystallization. String-like crystals firstly form columnar nuclei with the shape of straight chains, and lateral flakes with the shape of folded chains are grown at intervals on the centerline of the columnar nuclei [14]. Due to the characteristics of the dual structure, string crystals have high strength and strong corrosion resistance. Compared with oriented nuclei, it is found that oriented nuclei are more advantageous in the mechanical properties of polymer products and play an important role in the growth of string-like crystals. In the course of experimental studies, directed nucleation of polymers is often generated by flow induction or by the use of nucleating agents. The oriented nuclei

produced by nucleating agents are different from those produced under flow induction. The oriented nuclei produced by nucleating agents do not need to be matched with the polymer lattice and are mainly affected by the density of nucleation sites and the surface properties of the nucleating agent. Influenced by this, orientation-induced string crystals usually form a hybrid structure [15].

Due to the complexity of the hybrid structure, this paper only studies the oriented core of the polymer formed under flow induction and uses the dynamic growth model of polymer crystallization to carry out numerical simulation research on isotactic polystyrene. According to the distribution principle of the polymer lattice, the initial crystal nucleus is defined as a columnar crystal nucleus composed of 300 monomers [16]. In the simulation, the initial latent heat is $K_0 = 1.6$, the anisotropy strength is $\varepsilon = 0.06$, the anisotropy modulus is $j = 4$, and the numerical simulation obtains the skeletal morphology of isotactic polystyrene. The time iteration steps in Figure 7 are 1000, 3000, and 5000, respectively. (a–c) is the numerical result, and (d) is the microstructure of isotactic polystyrene observed under the high-power electron microscope. The simulation results are compared and analyzed with the experimental results observed under the high-power electron microscope, and we found that the numerical results were almost in good agreement with the experimental observations and verified the feasibility of the dynamic growth model of polymer crystallization.

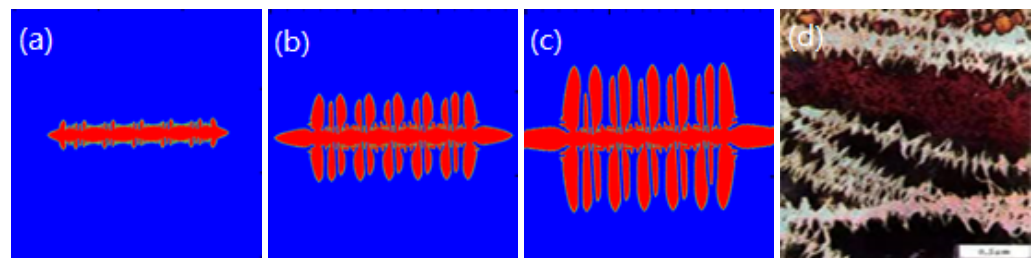


Figure 7. When $K_0 = 1.6$, the string crystals shape of is obtained by numerical simulation. ((a–c) are the numerical simulation results with time iteration steps of 1000, 3000 and 5000, respectively. (d) is the experimental result).

4.3. The Effect of Flow Rate on Polymer Crystallization

In order to verify the effect of convection on polymer crystallization, the numerical simulation results of pure diffusion and forced convection were analyzed and compared. This paper uses the dynamic growth model to numerically simulate the growth of isotactic polystyrene.

In the simulation, the initial latent heat is $K_0 = 1.25$, the anisotropy strength is $\varepsilon = 0.06$, and the time iteration steps are 1000, 2000, 3000, and 4000, respectively. Under pure diffusion conditions, the crystalline morphology (a–d) of the polymer and the corresponding temperature field (e–h) distribution are shown in Figure 8. Under the condition of pure diffusion, the flow velocity V is added to simulate the effect of convection on the growth of the polymer. Take $v_x = 0$, $v_y = 1.5$ (v_x, v_y are the components of the velocity V), and the flow direction is vertical downward. The distribution of the crystalline morphology (a–d) and the corresponding temperature field (e–f) of the object is shown in Figure 9 as follows:

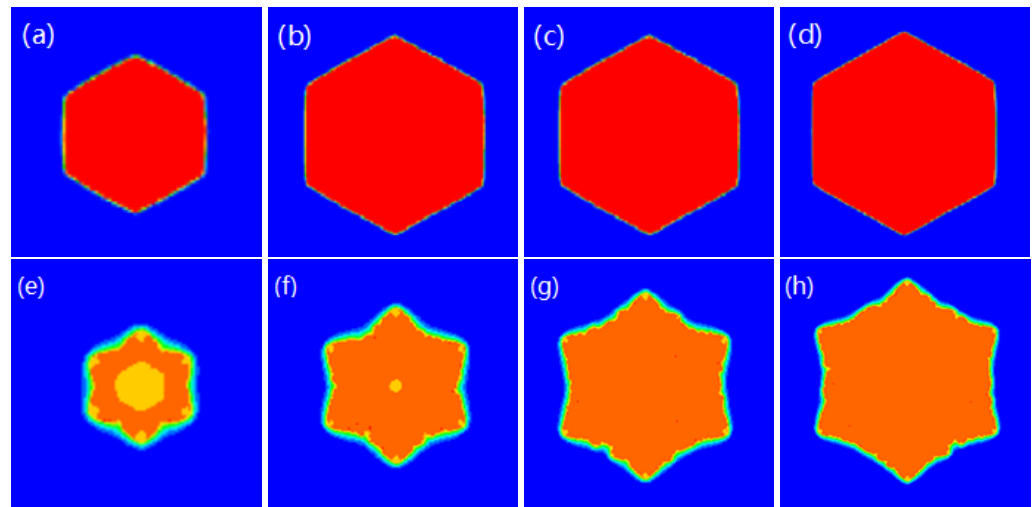


Figure 8. When $K_0 = 1.25$ under pure diffusion conditions, the simulated morphology of dendrites and the corresponding temperature field distribution. (Under pure diffusion conditions, (a–d) is the crystalline morphology of the polymer, and (e–h) is the corresponding temperature field).

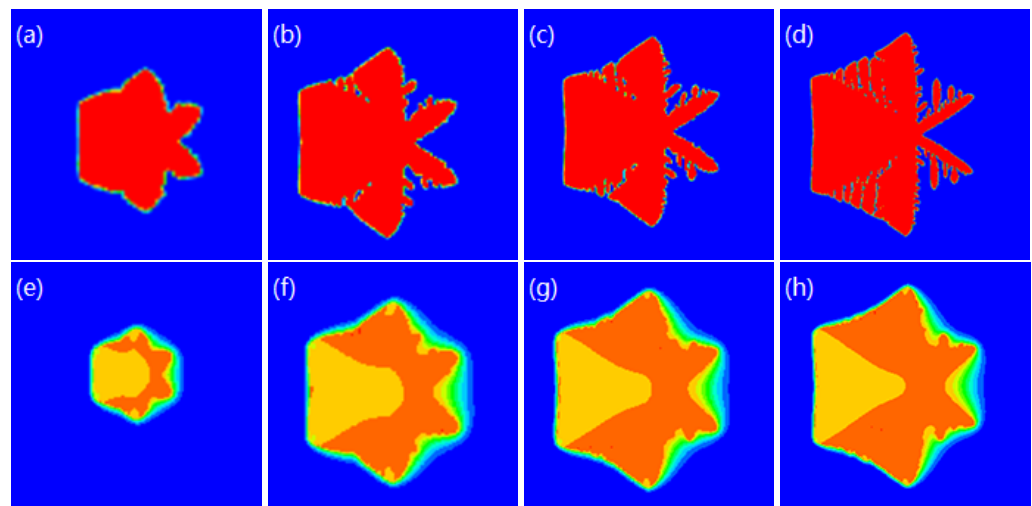


Figure 9. When $K_0 = 1.25$, $v_x = 0$, and $v_y = 1.5$, the simulated morphology of dendrites and the corresponding temperature field distribution affected by the flow velocity. ((a–d) is the crystalline morphology of the polymer after adding the flow rate and (e–h) is its corresponding temperature field).

In the simulation, the initial latent heat is $K_0 = 1.4$, the anisotropy strength is $\varepsilon = 0$, and the time iteration steps are 1000, 2000, 3000, and 4000, respectively. Under pure diffusion conditions, the crystalline morphology (a–d) of the polymer and the corresponding temperature field (e–h) distribution are shown in Figure 10. Under the condition of pure diffusion, add flow velocity V to simulate the effect of flow velocity on polymer crystallization, take $v_x = 0$, $v_y = 1.5$ (v_x , v_y are the components of velocity V), and the flow direction is vertical downward. The crystalline morphology (a–d) of the polymer and the distribution of the corresponding temperature field (e–f) are shown in Figure 11 as follows:

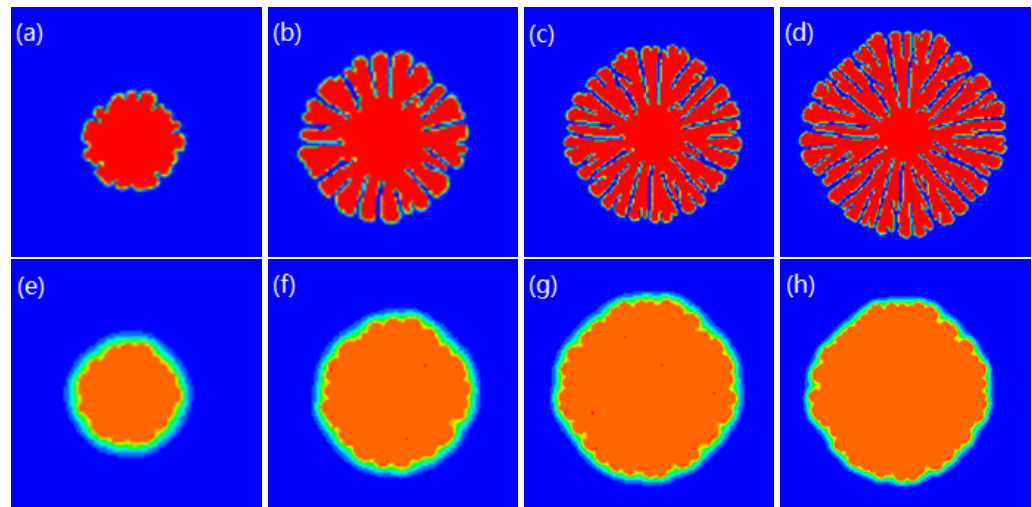


Figure 10. When $K_0 = 1.4$, under pure diffusion conditions, the morphology of the simulated spherulites and the corresponding temperature field distribution. (Under pure diffusion conditions, (a–d) is the crystalline morphology of the polymer, and (e–h) is the corresponding temperature field).

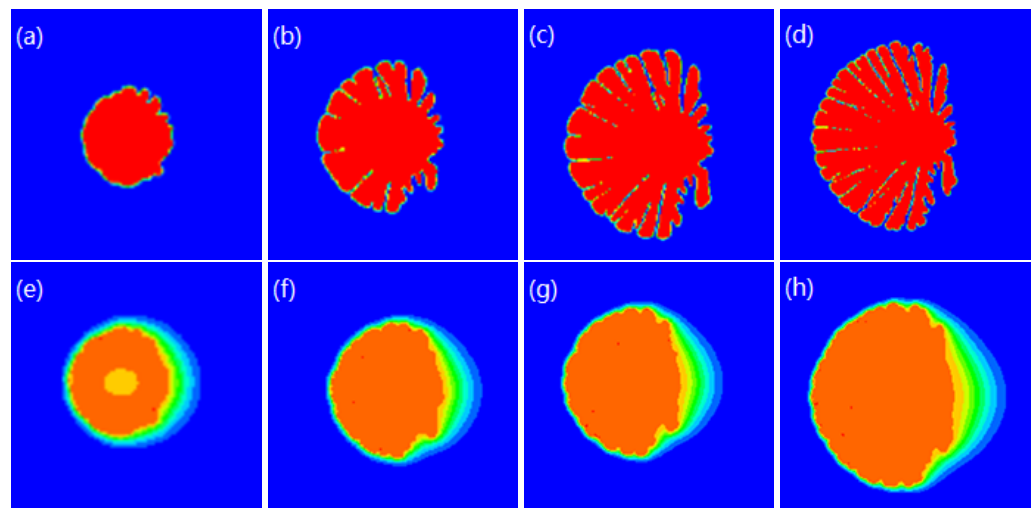


Figure 11. When $K_0 = 1.4$, $v_x = 0, v_y = 1.5$, the simulated spherulite morphology and the corresponding temperature field distribution affected by the flow velocity. ((a–d) is the crystalline morphology of the polymer after adding the flow rate and (e–h) is its corresponding temperature field).

In the simulation, the initial latent heat K_0 is taken as 0.8, and the anisotropy intensity is $\varepsilon = 0.06$, and the time iteration steps are 1000, 2000, 3000, and 4000, respectively. Under pure diffusion conditions, the crystalline morphology (a–d) of the polymer and the corresponding temperature field (e–h) distribution are shown in Figure 12. Under the condition of pure diffusion, add flow velocity to simulate the effect of flow velocity on polymer crystallization, take $v_x = 0, v_y = 1.5$ (v_x, v_y are the components of velocity V), the flow direction is vertical downward, and polymerization. The distribution of the crystalline morphology (a–d) and the corresponding temperature field (e–h) of the object is shown in Figure 13, as follows:

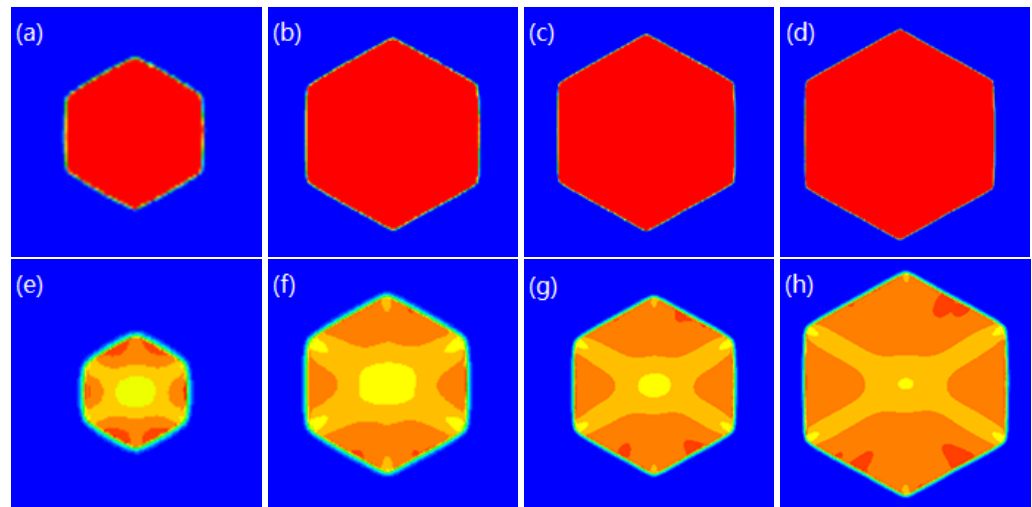


Figure 12. When $K_0 = 0.8$, under pure diffusion conditions, the simulated shape of spherulites and the corresponding temperature field distribution. (Under pure diffusion conditions, (a–d) is the crystalline morphology of the polymer, and (e–h) is the corresponding temperature field).

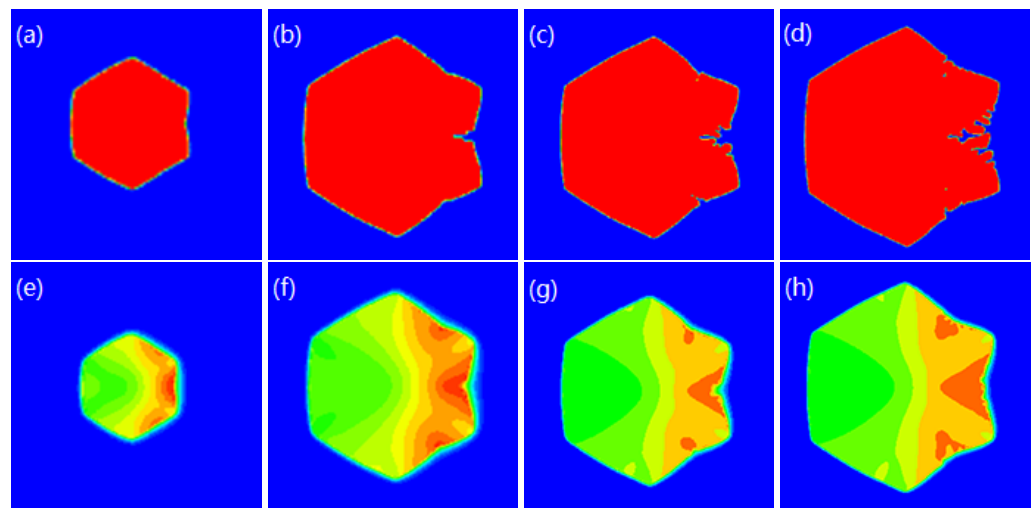


Figure 13. When $K_0 = 0.8$, $v_x = 0$, $v_y = 1.5$, the simulated shape of spherulites and the corresponding temperature field distribution affected by the flow velocity. ((a–d) is the crystalline morphology of the polymer after adding the flow rate and (e–h) is its corresponding temperature field).

5. Conclusions

Through the analysis and comparison of Figures 8–13, it is concluded that the temperature diffusion layer distribution around the polymer under pure diffusion conditions is uniform, and the morphology of the crystal shows a symmetrical trend. As time evolves, the main crystal arms gradually become thinner, and the side branches gradually become thicker and more numerous. After the flow rate V is added, the melt produces convection, and the temperature diffusion layer around the crystal is no longer uniform. The flow of the melt reduces the thickness of the temperature diffusion layer on the left, increases the actual undercooling of the polymer on the left, and promotes the growth of the polymer on the left. Forced convection causes the heat on the left and the release of solidification. The heat reduces the actual degree of supercooling of the polymer on the right side and inhibits the growth of the polymer on the right side.

Author Contributions: Methodology, B.Y.; software, B.Y.; validation, B.Y., Z.W. and Z.M.; formal analysis, Z.W.; writing—original draft preparation, B.Y.; writing—review and editing, B.Y.; visualization, Z.W. All authors have read and agreed to the published version of the manuscript.

Funding: This research was funded by the Natural Science Foundation of Shanxi Province, China (Grant No. 201901D111254).

Institutional Review Board Statement: There are no ethical issues involved in this study.

Data Availability Statement: Not applicable.

Acknowledgments: The authors thank the financial support of the Natural Science Foundation of Shanxi Province.

Conflicts of Interest: The authors declare no conflict to interest.

References

1. Zhang, C.H. Numerical Simulation Study of the Phase Field Method of Polymer Crystallization. Master's Thesis, Taiyuan University of science and Technology School, Taiyuan, China, 2016.
2. Xu, J.; Reiter, G.; Alamo, R.G. Concepts of nucleation in polymer crystallization. *Crystals* **2021**, *11*, 304. [[CrossRef](#)]
3. Ma, Z.B. Phase Field Model and Its Application. Master's Thesis, Nankai University, Tianjin, China, 2010.
4. Kobayashi, R. Modeling and numerical simulations of dendritic crystal growth. *J. Environ. Sci.* **1993**, *63*, 410–423. [[CrossRef](#)]
5. Gránásy, L.; Pusztai, T.; Tegze, G. Growth and form of spherulites. *Phys. Rev. E* **2005**, *72*, 011605. [[CrossRef](#)] [[PubMed](#)]
6. Gránásy, L.; Pusztai, T.; Warren, J.A. Modelling polycrystalline solidification using phase field theory. *J. Phys. Condens. Matter* **2004**, *16*, R1205. [[CrossRef](#)]
7. Xu, H.; Matkar, R.; Kyu, T. Phase-field modeling on morphological landscape of isotactic polystyrene single crystals. *Phys. Rev. E* **2005**, *72*, 011804. [[CrossRef](#)] [[PubMed](#)]
8. Harrowell, P.R.; Oxtoby, D.W. On the interaction between order and a moving interface: Dynamical disordering and anisotropic growth rates. *J. Chem. Phys.* **1987**, *86*, 2932–2942. [[CrossRef](#)]
9. Wang, X.D.; Ou, J.; Su, J. phase-field model for simulating various spherulite morphologies of semi-crystalline polymers. *Chin. Phys. B* **2013**, *10*, 387–393. [[CrossRef](#)]
10. Bahloul, A.; Doghri, I.; Adam, L. An enhanced phase field model for the numerical simulation of polymer crystallization. *Polym. Cryst.* **2020**, *3*, 182–207. [[CrossRef](#)]
11. Hoffman, J.D.; Lauritzen, J.I. Crystallization of Bulk Polymers with Chain Folding: Theory of Growth of Lamellar Spherulites. *J. Res. Natl. Bur. Stand. Sect. Phys. Chem.* **1961**, *65A*, 297. [[CrossRef](#)] [[PubMed](#)]
12. Hoffman, J.D.; Lauritzen, J.I.; Ross, G.S. On the growth rate of spherulites and axialites from the melt in polyethylene fractions: Regime I and regime II crystallization. *J. Res. Natl. Bur. Stand. Sect. Phys. Chem.* **1975**, *79A*, 671. [[CrossRef](#)] [[PubMed](#)]
13. Hua, D.H.; Li, X.G. *Numerical Solution of Differential Equations*; Publishing House of Electronics Industry: Beijing, China, 2008; pp. 7–8.
14. Wang, X.D.; Ou, J.; Su, J. Investigating the role of oriented nucleus in polymer shish-kebab crystal growth via phase-field method. *J. Chem. Phys.* **2014**, *140*, 4197. [[CrossRef](#)]
15. Yuan, X.F.; Ding, Y.T.; Ding, T.B. Phase field method of dendrite growth behavior under convection. *Chin. J. Nonferrous Met.* **2010**, *4*, 681–687.
16. He, C.C.; Yang, B.X. Simulation of dendrite growth of pure material under constant velocity flow field by phase field method. *J. Taiyuan Univ. Sci. Technol.* **2017**, *38*, 238–241.